Shake Before Use: Artificial Contrast Generation for Improved Space Imaging using Neuromorphic Event-Based Vision Sensors

Nicholas Owen Ralph, Darren Maybour, Alexandre Marcireau, Imogen Jones, Ain De Horta and Gregory Cohen

International Centre for Neuromorphic Systems, The MARCS Institute for Brain, Behaviour and Development, Western Sydney University

ABSTRACT

In this paper, we present a study into artificial contrast generation for neuromorphic event-based vision sensors as a novel approach to improve event-based space imaging and Space Domain Awareness. Event-based vision sensors are high-speed contrast-driven sensors that embrace the antithesis of conventional space imaging by exhibiting better detection and accuracy when tracking stability decreases. We demonstrate the performance of an artificial contrast generation system as a technique to improve the performance of an event-based space imaging system by introducing controlled motion into the incoming light path to artificially generate contrast and improve target signal. We show that artificial contrast generators can improve the target detection and the spatial resolving capabilities of an event-based space imaging system. This work represents the latest approach in neuromorphic engineering to solve real-world problems using mechanisms such as saccadic eye motion found in biological sensing for ocular fixation. By improving the performance of event-based space imaging systems, this sensor's unique capabilities can be further leveraged in SSA tasks to contribute to international SSA efforts and the development of novel space imaging techniques.

1. INTRODUCTION

Neuromorphic Event-based Sensors (EBSs) are biology-inspired visions sensors which attempt to replicate the function of biological photo-receptors [12] to detect changes in luminance instead of collecting image frames as in conventional image sensors. These sensors are characterised by an high temporal resolution, dynamic range, and low power consumption [6]. Unlike conventional frame-based cameras which synchronously reads an entire image frame for all pixels at regular intervals, EBSs detect per-pixel contrast change and report these changes asynchronously as 'events'. Each event, e, contains the image plane position, polarity of the contrast change and a micro-second time-stamp of when the event time occurred $e = (x, y, p, t)$. Demonstrated in Fig. 1, these events are only transmitted when contrast is detected, which results in significantly reduced data redundancy compared to frame-based cameras, which samples all pixels in every frame regardless of the scene activity. Externally controlled parameters set the contrast change threshold, as illustrated in Fig. 1. These biases affect the overall responsiveness of the EBS pixel array.

The EBS has been successfully demonstrated as a novel and effective approach to space domain awareness and space imaging [5] and as a technique capable of observing and characterising satellites with a significantly higher temporal resolution and lower output data volume than conventional frame-based sensors. As a comparison, conventional image sensors require exposure times, suffer from blur effects when observing moving targets and capture redundant information such as dark background sky.

Yet, the EBS suffers from the 'perfect tracking phenomena', where stars and satellites observed while tracking may only become visible with contrast generated either by mutual motion between the source and telescope, atmospheric seeing, or improper tracking. Without significant changes in the incoming light from a target, there may be little detectable contrast for the EBS, especially for faint targets. Drift scanning or leap-frog observing is often a solution to this dilemma, where a telescope will be positioned by the mount on sky region so that the target Resident Space Object (RSO) moves through the FOV rather than tracking it to maintain the target position in the FOV. However,

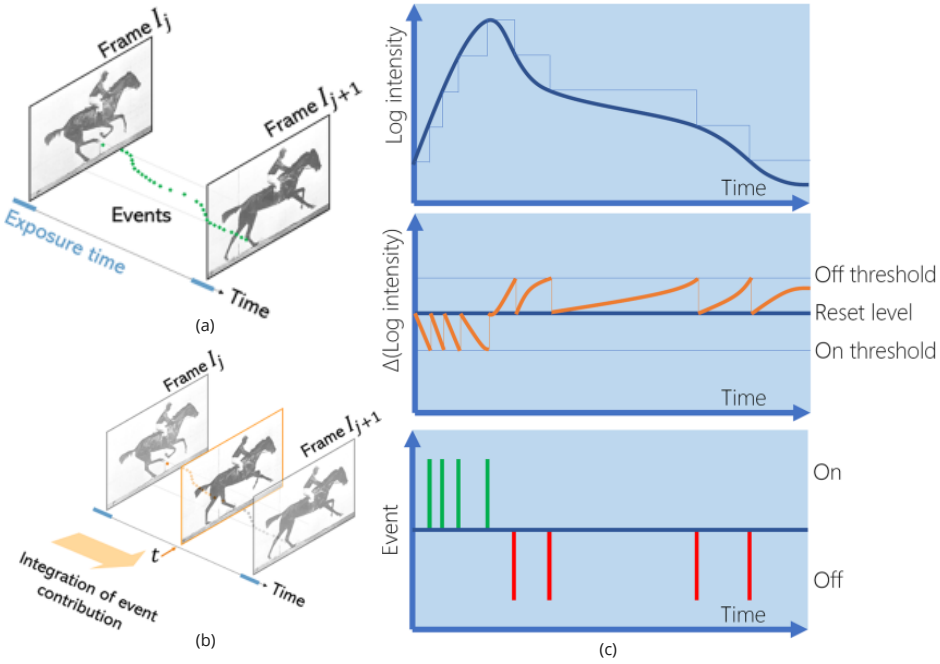

Fig. 1: Comparison of events and image frames (a), where an image frame captures a full frame of light intensities, an EBVS will detect only intensity changes as microsecond time-stamped events. In (b), the regular frame interval is apparent over time, while events occur asynchronously. In (c), the pixel operation of an event camera is demonstrated, where the log intensity received by a pixel over time is measured and compared to bias thresholds to produce events. From [2].

this approach reduces the time the target can be observed before it leaves the FOV, limiting the number of obtainable position measurements. Although counter-intuitive, a solution to this challenge and the balance between tracked observations and drift scanning is introducing a controlled mutual motion into the imaging system to generate additional detectable contrast. Due to the high-speed performance of these sensors, event-based space imaging systems can explore this alternate approach to space imaging with improved target detection without problematic motion blur.

In this paper, we draw inspiration from saccadic eye motion for fixation in biological vision systems [17] and develop Artificial Contrast Generators (ACGs) as a family of devices that induce mutual motion in the EBS to visualise an otherwise static scene and improve target detection. We present two proposed devices which are designed to be installed between a given telescope and the EBS:

1. The Mirrored-ACG, a 2-axis beam steering system using galvanometer mirrors which generate contrast by translating incoming light from the telescope across the EBS focal plane with a known pattern and frequency,
2. The Lensed-ACG, a variable focus system that uses a Corning Varioptic liquid lens to rapidly cycle the focal length of the image plane at a precise range and frequency with optimal focus at an arbitrary point within the focal length travel. The Lensed-ACG generates contrast by quickly refocusing sources to trigger events as their extent cycles between growing and shrinking over surrounding pixels.

These proposed contrast generators are designed to use induce spatio-temporal features on the image plane with a known direction and magnitude. This motion forms a prior allows actual emission from real radiation sources and targets to be more easily differentiated from random noise through the correlated motion. Using these ACGs, target detection algorithms can be improved by incorporating a prior on the expected spatio-temporal features using the known beam steering pattern. Contrast generation using an ACG can also produce significantly more position samples of a target through the additional induced events, which can be used to estimate a more accurate sub-pixel target positions. By steering oncoming light across multiple pixels, the overall amount of collected light can be increased by

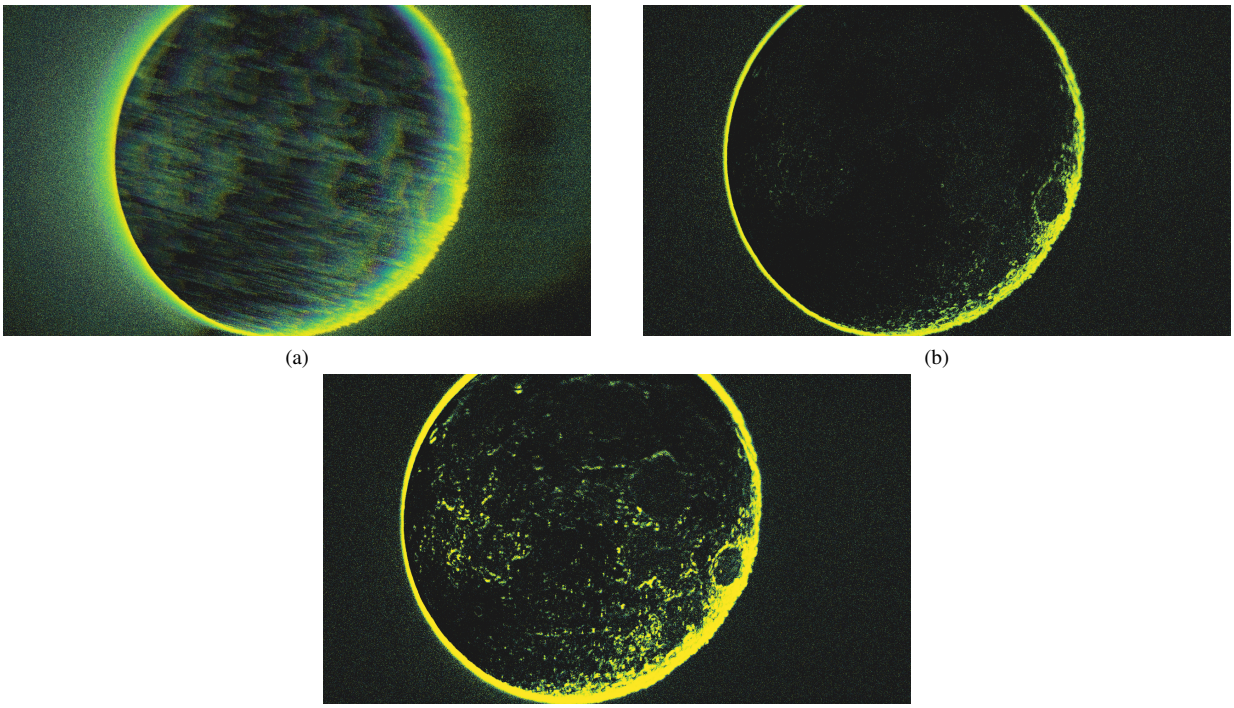

(a) (b)

(c)

Fig. 2: EBS accumulated event observations of the moon using the wide Field-of-View (FOV) small aperture Western Sydney University (WSU) finder-scope using drift-scanning with no sidereal tracking (a), during tracking (b), and during tracking with both axis of the Mirrored Artificial Contrast Generator (M-ACG) active using 400 mVpp 60 Hz sine wave inputs with a 90 degrees phase difference, steering the beam slightly in an elliptical manner (c), demonstrating the M-ACG's ability to generate sufficient contrast to resolve the features of the tracked moon an otherwise static target.

reducing the likelihood of light falling between pixels on the array. The possibility of incoming light straddling the pixels and reducing the overall light collected by a single pixel is an issue shared among all optical sensors with pixel arrays and non-negligible fill factor [18] which is addressed in this work.

In the wider neuromorphic community, techniques for basic contrast generation have been proposed for terrestrial tasks such as texture enhancement with circular beam steering on the focal plane using a rotating prism [9], and cyclic focusing for depth estimation using liquid lenses [13] [8]. Contrast generation has also been demonstrated using ego-motion (mutual motion) induced by a moving EBS platform for motion segmentation by de-correlating the known motion of a locomotive imaging platform [14]. Similarly, ego-motion on a pan-tilt mount akin to biological saccadic eye motion to generate contrast for a spike-based recognition system [15]. In event-based space imaging, drift scanning has been used as a method to generate contrast for stars and RSO in real-world data [4], [16] and in physically simulated data [3], [1] by using telescope mount motion, motion of the target itself, or sidereal motion as a contrast source. The results presented here are the first observations produced with these devices and any similar devices for space imaging and astronomy.

2. METHODOLOGY

In this paper, we propose the Mirrored-ACG, a device to generate contrast by 'beam steering' incoming light across the EBS image plane, and the Lensed-ACG, a device to rapidly focus and de-focus light on the EBS image plane. We evaluate these devices using real-world observations of extended objects, dense star-fields and RSOs. Utilising these real-world observations, we explore different ACG configurations with a range of beam steering patterns and observing techniques to evaluate the devices based on detected source counts and source extents for target resolving.

(a)

(b)

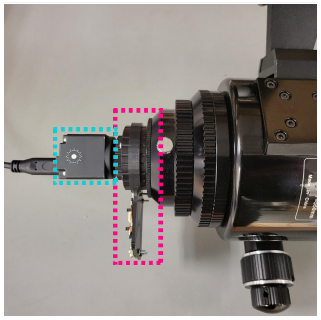

(c)

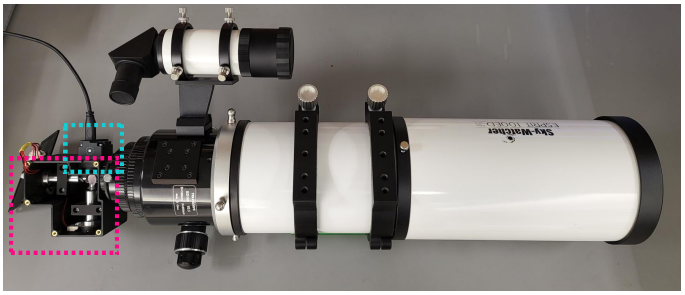

(d)

Fig. 3: The Astrosite-1 observatory (a), the EBS (Prophesee Gen 4 HD - EVK4) with a telephoto lens (b), the Lensed Artificial Contrast Generator (Lensed-ACG) in (c) and Mirrored Artificial Contrast Generator (Mirrored-ACG) in (d) each labelled with a dashed magenta rectangle mounted between the 6" refracting telescope detailed in Tab. 2 and the EBS labelled with a dashed cyan rectangle.

2.1 Data Collection

To validate the performance of the ACG and study the effect on the event-data, we assess the ACGs using the latest generation Prophesee Gen 4 HD (EVK4) (specifications specified in Tab. 1 and various optical telescopes (summarised in Tab. 2). In all experiments, the respective ACG is mounted between the telescope and the EBS focal plane. Observations using an EBS are generally conducted using wide FOV telescope imaging systems to avoid known challenges with narrow FOV optics where the contrast is reduced as a narrow FOV will result in source Point Spread Functions (PSFs) spreading over a larger region compared to wider FOV telescopes [16]. The ACGs were tested using 10-second observations of a star-field (a collection of point sources), the moon as a bright extended source, and an RSO. The 'Jewel Box', an open star cluster (Kappa Crucis Cluster NGC 4755) was chosen as the candidate star-field

as it contains many sources with various brightness and individual proximity. A variety of configurations for the ACGs were tested to determine the ideal beam steering displacement and speed for the Mirrored-ACG and the combination of cyclic focus range and speed for the Lensed-ACG. For each star-field and moon observation conducted while the ACG was active, two baseline observations were also recorded: an observation while the respective ACG was inactive and tracking the given target, and an observation also with the inactive ACG but without source tracking. All RSO observations were performed using mount tracking to maintain the target position in the FOV for the duration of the observation.

2.2 Mirrored and Lensed Artificial Contrast Generator Design

The ACGs are prototype devices developed at the International Centre for Neuromorphic Systems (ICNS) as a first-principles test for contrast generation in event-based space imaging systems. The design focus of the ACG devices are:

- Accurate and repeatable beam steering control with minimal (unintended) distortion,
- Robust to operating conditions and orientation,
- Compact to ensure the added distance between the telescope and EBS fits within the back-focus of most telescopes.

These factors preclude simple vibration systems for artificial contrast generation using the EBS. Our previous work has shown that the additional random high-speed and high-frequency vibration and resulting motion of the mount induced by windy conditions reduces the sensitivity of the EBS [16]. For this reason, a similar vibration of the EBS will induce neither precise nor known motion, which is both difficult to compensate for and will reduce the detectable source count for faint sources. Here, we present two approaches to contrast generation with beam steering via translation using the Mirrored-ACG, and variable focus using the Lensed-ACG.

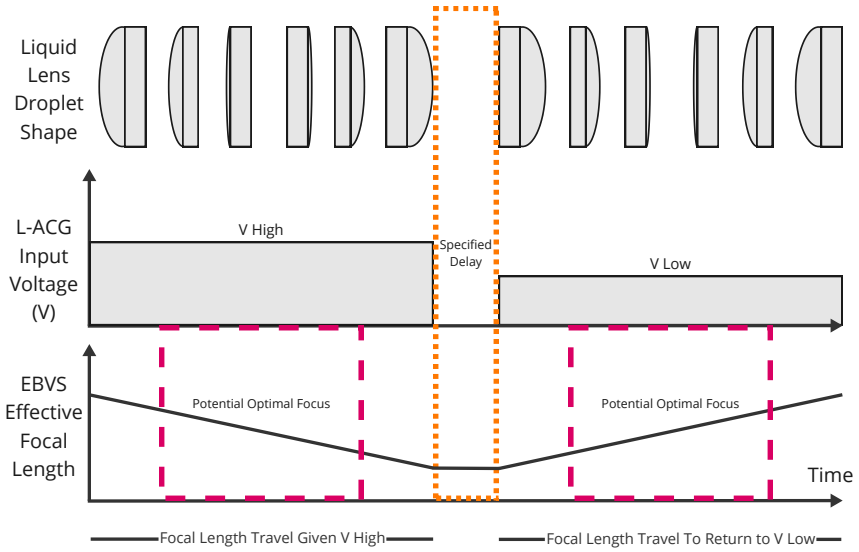

Fig. 4: Demonstration of the Lensed-ACG foal length travel. With the input voltage set to V high, the initial effective focal length changes as liquid lens droplet shape transforms, resulting in a new effective focal length after a response time of approximately 10 ms. After the specified delay (1 second at the lowest for our experiments), the liquid lens returns to the original shape and focal length with the V low input. Optimal focus is reached at some stage in each focal length travel.

The Mirrored-ACG is a prototype based on a standard 2-axis 'galvo-mirror' beam steering system as illustrated in Fig. 5. A galvo-mirror is a typical galvanometer, comprising a spring-loaded coil which rotates within a magnetic field when current passes through the coil. In a galvo-mirror, a mirror is mounted on the central shaft where the coil

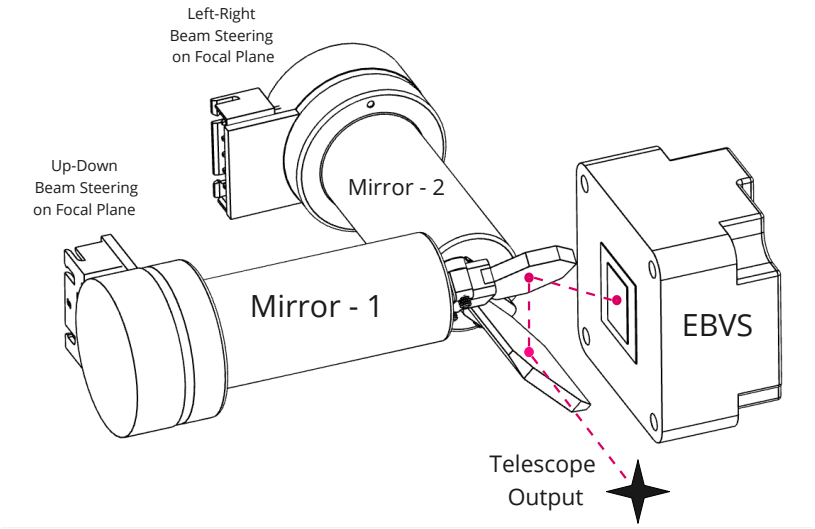

(a)

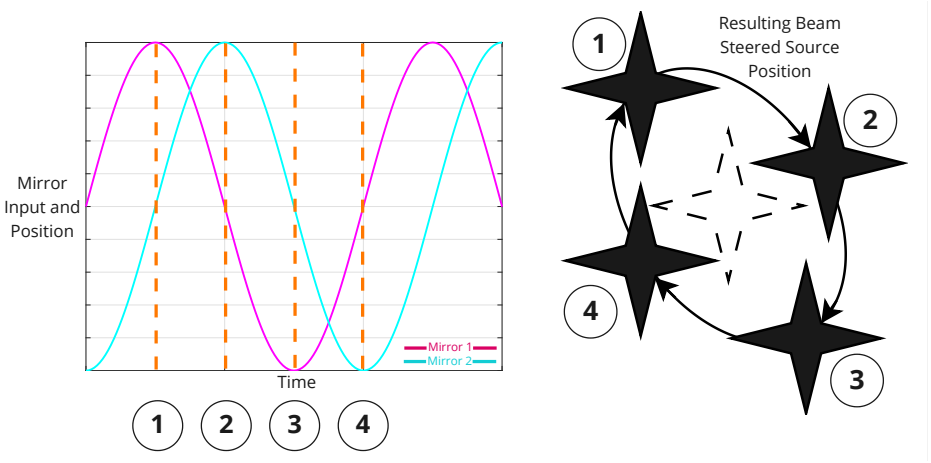

(b)

Fig. 5: Simplified render of the Mirrored-ACG (a), illustrating the beam steering action, where incoming light from the telescope is reflected from each galvo-mirror onto the EBS image plane. Mirror 1 and mirror 2 are responsible for 'up-down' and 'left-right' translation of the beam respectively. The resulting motion with a sine wave input to both mirrors at a 90-degrees phase difference causes sources to appear as if they were moving in circular pattern (b), however without closed-loop control, the pattern becomes roughly elliptical and the angle of each galvo-mirror is roughly proportional to the input voltage.

is wrapped. The Mirrored-ACG contains two rotating galvanometer-mounted mirrors oriented at 45 degrees from one another such that oncoming light at the telescope focal plane reflects from the first mirror onto the second and then to the EBS. The rotational axis of the mirrors is perpendicular so that the combined control of both mirrors can steer the incoming beam in two dimensions. The input to the Mirrored-ACG is a signal such as a a sine or square wave, which we tested with various peak voltages in the range of 200-700 mVpp, and frequencies ranging 1-60 Hz (maximum frequency for our particular galvo-mirrors). The angular displacement of each galvo-mirror is proportional to the input voltage. The galvo-mirrors are not currently implemented using closed-loop control. All tests using the Mirrored-ACG use the same peak-peak voltage for both mirrors. The beam displacement caused by peak voltages within this range is not easily determined without a closed-loop controller, however, the minimum obtainable motion for a full sweep in a single axis was less than 5 pixels using a 200 mVpp sine wave at 1 Hz. In a 1-axis configuration, a single mirror can be driven for motion in one direction. In the 2-axis configuration, a sine wave input for each mirror

with a 90-degree phase difference can drive the beam in an elliptical pattern to generate contrast from all directions of a given source's 'edges'. Likewise, we can use a square wave with a 90-degree phase difference to move the source features in a square pattern (up-left-down-right, generally with curved corners in the absence of a closed-loop controller).

In our exploration of artificial contrast generation, we also developed the Lensed-ACG prototype illustrated in Fig. 4 as an optical system with a variable focal length placed between the telescope and the EBS to generate contrast by changing the focus of the EBS as a target PSF spreads across nearby pixels. The Lensed-ACG houses a voltage-driven Corning Varioptic variable focus liquid lens with focal length travel, which is approximately linearly proportional to an input voltage between 30-75 V using this particular lens, with a range of -5 to +15 dioptre.

In the centre of a liquid lens is a transparent droplet. A liquid lens uses electrowetting to rapidly and precisely change the surface shape of the droplet using an electric field. As the surface curvature of the transparent liquid changes, so does the effective focal length of the lens assembly. By varying the input voltage, we can rapidly change the focal length of the EBS (with a response time of 10 ms). Without mechanical parts, we avoid technical challenges such as lash, wear and additional vibration. The expected change in the spatial extent of sources caused by the focus change is challenging to estimate as the spatial extent is also based on source brightness. Regardless, we expect bright sources to rapidly grow and shrink. Conversely, faint sources will appear as highly compact sources as they appear at optimal focus.

Using a square wave input, we control both the focal length travel and the start time of the focal length change, which we encode as the pulse peak and duration. The Lensed-ACG generates contrast in the EBS by rapidly refocusing sources to spread sources over surrounding pixels as the focal length increases past the optimal focus and then shrinks as it approaches optimal focus before returning to the unfocused position. The Lensed-ACG will always locate the optimal focus while ever it is within the focal length travel range of the lens, which addresses the challenging problem of obtaining the proper focus for an EBS for precise imaging of distant point sources. In future work, we will explore more continuous focal length travel, potentially in a closed-loop fashion to automatically generate contrast around the optimal focus.

2.3 Data Analysis, Post-processing and Filtering

The event data from each observation is displayed in accumulated frames using colour-time plots[1] where events are accumulated and colour-coded, where the intensity and opacity of events are proportional to their recent activation. All observations are cropped with a pixel mask over the outer 100 pixels on the field to remove artefacts caused by blurring on the field edges using the Mirrored-ACG and spherical distortions using the Lensed-ACG due to the relatively small clear aperture of the current prototype. Additional filtering is performed to remove hot pixels and single isolated pixels before the source finding step using a median filter with a 3×3 kernel. The collected data are post-processed without any compensation for the motion of the respective ACG. Development of ACG compensation algorithms will be a key focus in future studies.

Detected source count and source extent are used as metrics to examine the performance of the ACGs. These statistics are estimated using the source finder in Astrometry.net; 'Image2xy' [10]. In this preliminary study, sources are detected but not yet catalogue matched to their real-world sources, however in future work, detected sources will be correlated with the real-world star of their origin to confirm their validity and to relate their photometric characteristics with their detected spatio-temporal features. Source extent is used as a performance metric to quantify the compactness of event sources, determining how well the ACGs can resolve sources and the accuracy of source centroid estimates.

In drift-scanning observations, sources appear as spatio-temporal streaks moving through the FOV. These streaks can be 'warped' to collapse them along their trajectory into features that resemble the underlying point source PSF. These new motion compensated 'event sources' now comprise an event star map. For all drift-scanning observations, we use event-warping to create an event star map by estimating and compensating for the sidereal field motion in the observation. There are several techniques to estimate the field velocity for field motion compensation have been used, for event-based space imaging, ranging from manual techniques [4] to tracking [3] [1][16] and with methods such as Contrast Maximisation (CMAX), which is commonly used in the wider neuromorphic vision field. We use CMAX in this paper to estimate point trajectories (as the field velocity) in the event data by maximising a objective function optimisation function or metric for the compactness of warped features. Pixel variance is a well-accepted objective function for CMAX [7], among other simple methods and 'reward functions' such as maximum accumulation of

[1] from `https://github.com/neuromorphicsystems/charidotella`

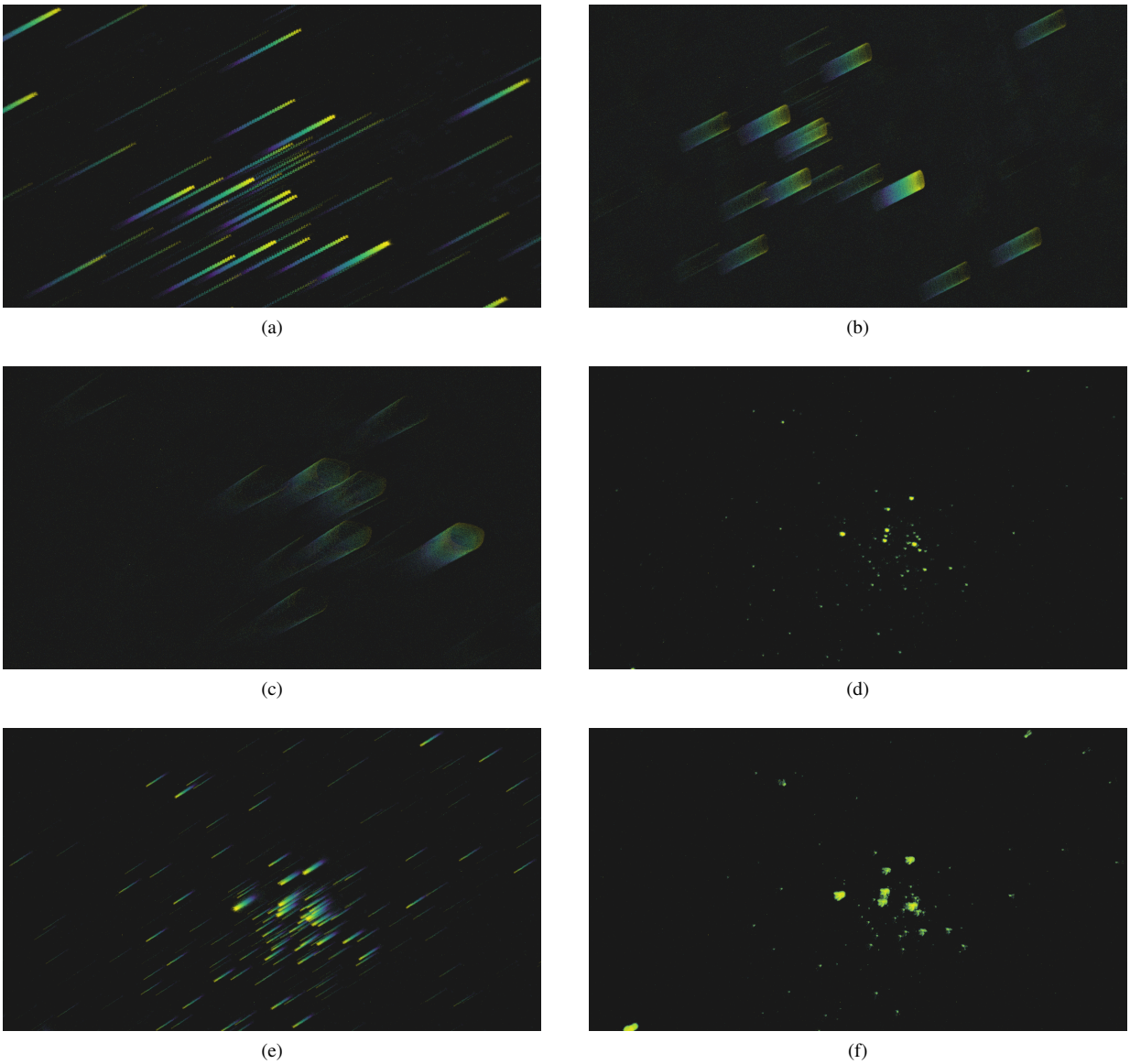

(a) (b) (c) (d) (e) (f)

Fig. 6: Various 2D Mirrored-ACG observations and beam steering patterns using square waves at 50% duty cycle and sine waves with varied peak and frequency and a 90-degree phase difference(a-c). In (a) subtle and high-speed elliptical beam steering with 100 mVpp at 60 Hz, (b) higher eccentricity elliptical beam steering but at a lower speed with 200 mVpp at 1 Hz, and (c) rounded edge square beam steering at high speed with 400 mVpp at 60 Hz. In (d-f), Lensed-ACG star-field observations with the Lensed-ACG inactive in (d) with mount tracking and (e) with drift scanning, and (f) with the Lensed-ACG active while mount tracking at 30-40 V at 2 Hz.

pixel values on the warped image [19]. In addition to drift-scanning observations, we use CMAX to compensate for the motion of the Mirrored-ACG given that the translation of sources on the focal plane is simply an additional point trajectory that can be compensated. The Mirrored-ACG motion must be compensated since the additional beam steering motion will not permit point source detection in Image2xy as the motion induced spatio-temporal features of event sources do not resemble compact PSFs as the source finder expects.

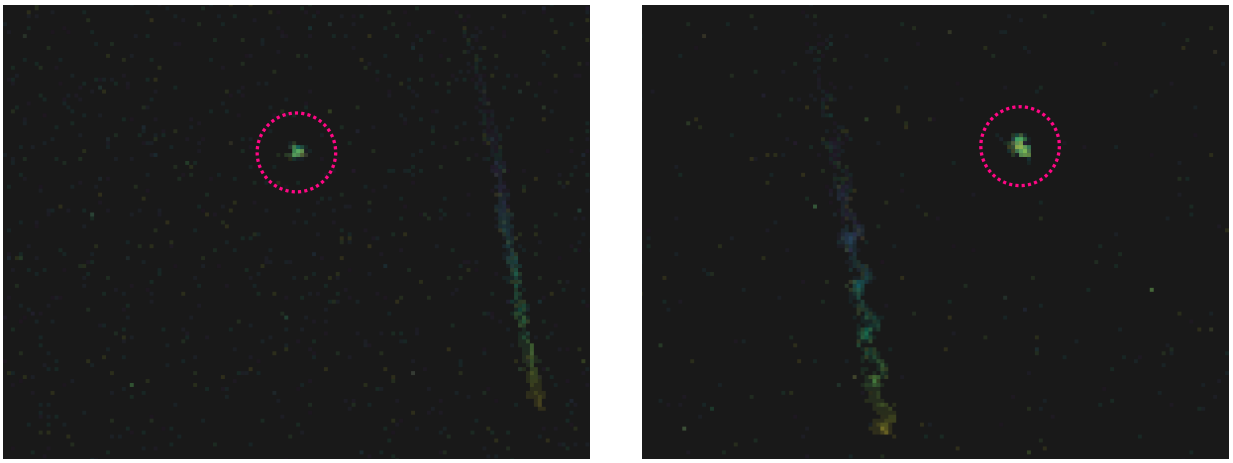

(a) (b)

Fig. 7: Tracked observations of the RSO ARIANE 5 R/B (NORAD ID: 28948) over 10 seconds labelled with a dashed magenta circle with a nearby star passed in both recordings, seen as a steak near the tracked source. In (a), we show a colour-time accumulated event frame of observations with the Lensed-ACG inactive. The tracked RSO generated 123 events over 13 pixels in this observation. In (b), an observation of the same RSO, but with the Lensed-ACG active with a short and low-speed focal length travel driven from 30-40 V at 2 Hz, the tracked RSO produced 326 events over an area of 36 pixels. These observations demonstrate the significant improvement to the RSO event count using the Lensed-ACG, in addition to a slight blurring of the point source at the extreme of the Lensed-ACG de-focus.

Table 1: Specifications of the Prophesee Gen 4 HD EBS used in this study [6].

Camera	**Resolution (pixels)**	**Latency (μs)**	**Dynamic Resolution (dB)**	**Min Contrast Sensitivity (%)**	**Chip Size (mm^2)**	**Pixel Size (μm^2)**	**Fill Factor (%)**
Gen 4 HD	1280×720	20-150	> 124	11	6.2×3.5	4.86×4.86	> 77

Table 2: Telescope specifications and experiments used to test the ACGs using wide FOV telescopes to increase per-pixel contrast by 'confining' sources to fewer pixels. Pixel scale assumes square pixels and array.

Telescope	**Observations**	**Aperture (mm)**	**Focal Length (mm)**	**EBVS Image Plane FOV (arcmin)**	**EBVS Pixel Scale (arcsec/pix)**
Astrosite-1 RASA	Star-field, RSO	279	620	34.49×19.41	1.617
Portable Sky-Watcher 6" Refractor	Star-field (no-sidereal tracking)	152.4	550	42.77×24.06	1.822
WSU Observatory Finder-Scope 3" Refractor	Lunar	76.2	500	38.88×21.88	2.005

3. RESULTS AND DISCUSSIONS

The results presented here are the first observations produced with these ACG devices and any similar devices for space imaging and astronomy. These devices initially required significant testing, which was subject to telescope availability and weather. As a result, no RSO observations were collected using the Mirrored-ACG. Further development with these devices will involve more numerous observations under more conditions will be collected, such as RSO observations with the Mirrored-ACG and lunar tracked observations and drift scanning with the Lensed-ACG

3.1 M-ACG Results

The Mirrored-ACG was tested with observations of the moon as a bright and extended object in Fig. 2 using the large FOV, small 3" aperture finder-scope (Tab. 2). Using colour-time event accumulations, we show that drift-scanning alone produces blurred image features, which requires motion compensation to create a coherent image. Drift scanning also eventually results in the target moving out of the FOV. In the tracked observation, we keep the moon in the FOV; however, this results in little detectable contrast from the moon's features, causing events to occur mainly around the apparent edge of the moon. However, we demonstrate the successful operation of the Mirrored-ACG (with a relatively low beam displacement at 400 mVpp) resolves the inner features of the otherwise static moon. Modifications must be made to CMAX before it can be used effectively to image the moon using drift-scanning as a large, bright, extended object that produces many events. Similarly, the Mirrored-ACG requires an optimisation to deconvolve the beam steering motion and resolve finer features. Regardless, the Mirrored-ACG as a device to permit the imaging of tracked targets is demonstrated.

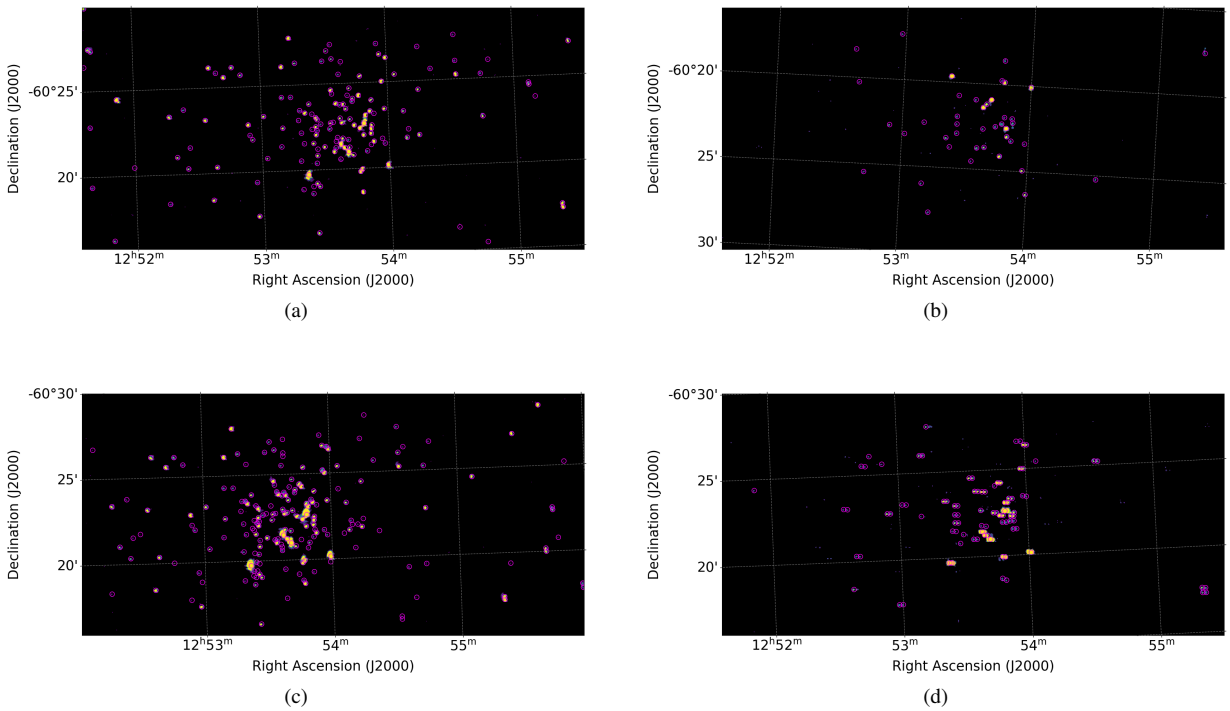

Fig. 8: Star-field experiments displayed using colour-time event accumulation with detected sources circled in magenta. In (a), a drift-scanning observation using CMAX motion compensation while the Mirrored-ACG is inactive, and in tracked observations with the Mirrored-ACG inactive (b). In (c), the Mirrored-ACG is active in the 1-axis configuration with a small and low-speed displacement beam steering pattern using sine wave at 200 mVpp 1 Hz and compensated CMAX. In (d), we show the same Mirrored-ACG settings with CMAX on a tracked observation. These results demonstrate that drift-scanning and tracked observations with the Mirrored-ACG significantly increases the source count compared to regular observations. Both Mirrored-ACG observations require CMAX for motion compensation, which causes source duplication in the tracked observation, however, Fig. 10 shows the field still contains more than twice the number of sources.

In our Mirrored-ACG star-field observations using 2-axis beam steering patterns with the 6" refractor telescope (Tab. 2), we induced several patterns with varying peak voltages and frequencies. Firstly, subtle and high-speed elliptical beam steering with 100 mVpp at 60 Hz, larger eccentricity elliptical beam steering but at a lower speed with 200 mVpp at 1 Hz, and rounded edge square beam steering at high speed with 400 mVpp at 60 Hz. No clear advantage was found with using square wave beam steering patterns. It was found that CMAX could motion compensate for the beam steering motion of the Mirrored-ACG data. Furthermore, this CMAX step appeared to be a requirement since the Image2XY source finder could not easily differentiate sources without compensation. Overall, these first tests

indicated that large beam displacement and speed significantly reduced the sensitivity of the EBS with an immediate and visible reduction in the number of detected sources.

Following these tests, we constrained our experiments to a single mirror at lower beam steering speeds and frequencies. In these 1-axis Mirrored-ACG tests at the lowest-beam steering displacement (200 mVpp) and a frequency of 1 Hz, we observe our best result regarding detectable source count. In Fig. 8, we demonstrate star-field experiments with the Mirrored-ACG active using this sine wave input with CMAX and observations with the Mirrored-ACG inactive for drift-scanning and tracked observations. These figures and the results shown in Fig. 10 suggest that both drift-scanning and tracked observations with the Mirrored-ACG significantly increase the source count compared to regular observations. Furthermore, Mirrored-ACG observations are shown with a consistently lower mean source extent, suggesting the Mirrored-ACG was able to resolve more sources with more compact features and the potential for lower centroid estimation error. Source duplication in the tracked observation is apparent in Fig. 8, but the results in Fig. 10 show that the field still contains more than twice the number of sources. Also illustrated is a general trend for all observations and techniques to increase in extent as the frame duration increases.

With additional events (effectively position samples) for the target motion and beam steering motion, we find more accurate CMAX motion estimation and, therefore, more accurate motion compensation. This improvement is indicated by the Mirrored-ACG CMAX motion compensation collapsing the beam steering spatio-temporal features onto compact point sources with a lower mean spatial extent than the regular drift scanning observation with CMAX. With this lower spatial extent, we see an increase in the resolving capabilities of the EBS in addition to a potential reduction in source confusion. Mirror miss-alignment and non-planar alignment of the EBS have adversely affected the observations when the Mirrored-ACG was a part of the imaging setup. These effects likely reduced the detectable source count of the star-field drift scan observations with sub-optimal focus.

3.2 L-ACG Results

Similar to the early Mirrored-ACG observations, the first Lensed-ACG tests revealed that the full range of the focal length travel and high-frequency focus change resulted in a reduction to the sensitivity of the EBS with a visible decrease in the number of detected sources. Following these early tests, we found the smallest visually detectable focus variation range of 30-40 V at 2 Hz (1 second delay between focal range return) yielded the greatest detectable source counts. In Fig. 9, we show colour-time accumulated event plots of star-field observations using the Lensed-ACG with this focus variation range and delay. These observations demonstrated that the Lensed-ACG (without a compensation algorithm) significantly increases the source count compared to regular tracked observations. However, the CMAX motion compensated drift-scanning observation with the Lensed-ACG inactive contained more sources. It is noted that discrepancies in source count can also be found due to slight differences in the field centre due to incorrect centring during observation. Further work is required to improve the Lensed-ACG and build a compensation algorithm to surpass the source count of the motion-compensated drift-scan recording and to only accumulate events near or at the optimal focus. In Fig. 7, we demonstrate the Lensed-ACG for tracked observations of RSO ARIANE 5 R/B (NORAD ID: 28948). In these observations with the Lensed-ACG active, a significant increase in the number of events over a larger area than the regular tracked observation was observed. With sources producing more events, targets can be analysed statistically to estimate a sub-pixel target position. Since the RSO is relatively bright, we observe an overall increase in the source extent at the peak of the de-focus. Overall, the Lensed-ACG is shown in these star-field observations and RSO observations to outperform regular tracked observations in terms of source count.

Although we see blurring from brighter sources, faint sources are better resolved with a smaller mean extent as they produce most of their events while the EBS is at or near optimal focus. Since the faint sources are more numerous, the mean source extent is still smaller than in observations with the Lensed-ACG inactive. These results are confirmed in Fig. 10, where observations with the Lensed-ACG have a lower mean source extent than regular observations. The Lensed-ACG can likely resolve faint sources well since they are only visible when the EBS is at or near optimal focus, which is also when they appear at their most compact. In Fig. 10, the performance of the Lensed-ACG has an immediate improvement at 0.5 seconds of observing compared to regular tracked observing. However,the benefit becomes less significant at longer exposure times with more integrated events with both active Lensed-ACG and inactive Lensed-ACG tracked observations containing a similar number of detected sources.

For both ACGs, we we conclude that,

1. The proposed ACG devices are an effective solution to the perfect tracking problem with a clear increase the contrast of sources and the detectable source count using the Lensed-ACG for tracked observations also for both

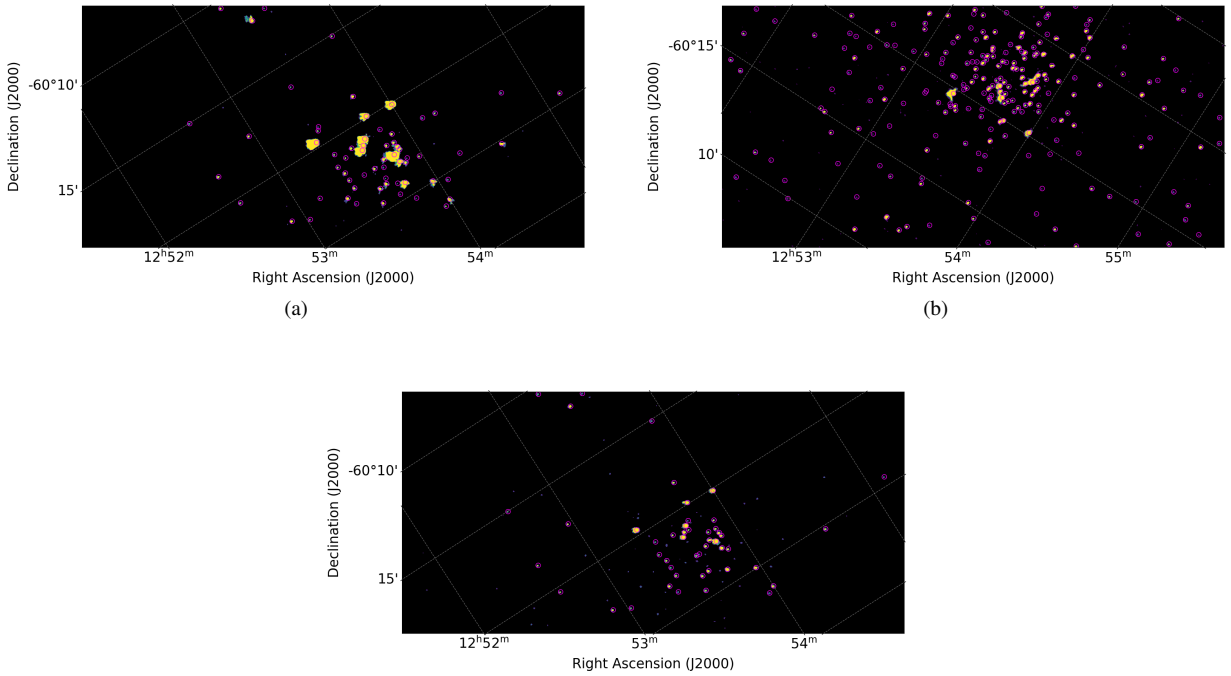

Fig. 9: Star-field observations of a CMAX motion compensated with detected sources circled in magenta. In (a), drift scanning observations with the Lensed-ACG inactive compared with tracked observations with the Lensed-ACG inactive (b), and (c) while the Lensed-ACG is active with a short and low-speed focal length travel driven from 30-40 V at 2 Hz. These results demonstrate that the Lensed-ACG without a compensation algorithm significantly increases the source count compared to regular tracked observations but fewer sources than the CMAX motion-compensated drift-scanning observation.

drift-scanning and tracked observations using the Mirrored-ACG,

2. The ACG devices generally reduce the source spatial extent with more resolved sources, which reduces the overall source centroid estimation error, resulting in a higher spatial resolution (with the exception to bright sources while using the Lensed-ACG),
3. For the Mirrored-ACG specifically, we see an improvement in both drift scan and tracked observation regimes, with the best results when combining Mirrored-ACG with drift scanning and CMAX.
4. The Mirrored-ACG can use CMAX to compensate the beam steering action with better performance than CMAX with regular drift-scanning, but a specialised algorithm has not been developed.
5. The Lensed-ACG can automatically locate the EBS optimal focus by sweeping through a range of focal lengths which reveals faint and well resolved sources.

Although the Lensed-ACG did not surpass the source count of the drift-scanning CMAX motion-compensated event data, it still surpassed the performance of regular tracked observing, which is generally required for RSO observation. Additionally, we can expect that a similarly well-studied and optimised algorithm for motion-compensating drift-scanning observations would significantly improve the performance of the ACGs. The Lensed-ACG was shown to allow the EBS to cyclically reach optimal focus once for each focal length travel, which has a known and constant frequency that could be used as a prior in a compensation algorithm to integrate events specifically when the Lensed-ACG is generating events at the optimal focus.

CMAX and tracker-based event warping has been demonstrated as an effective approach to deconvolving mount motion in drift scanning. However, an algorithm specifically to compensate for the induced motion of the ACGs

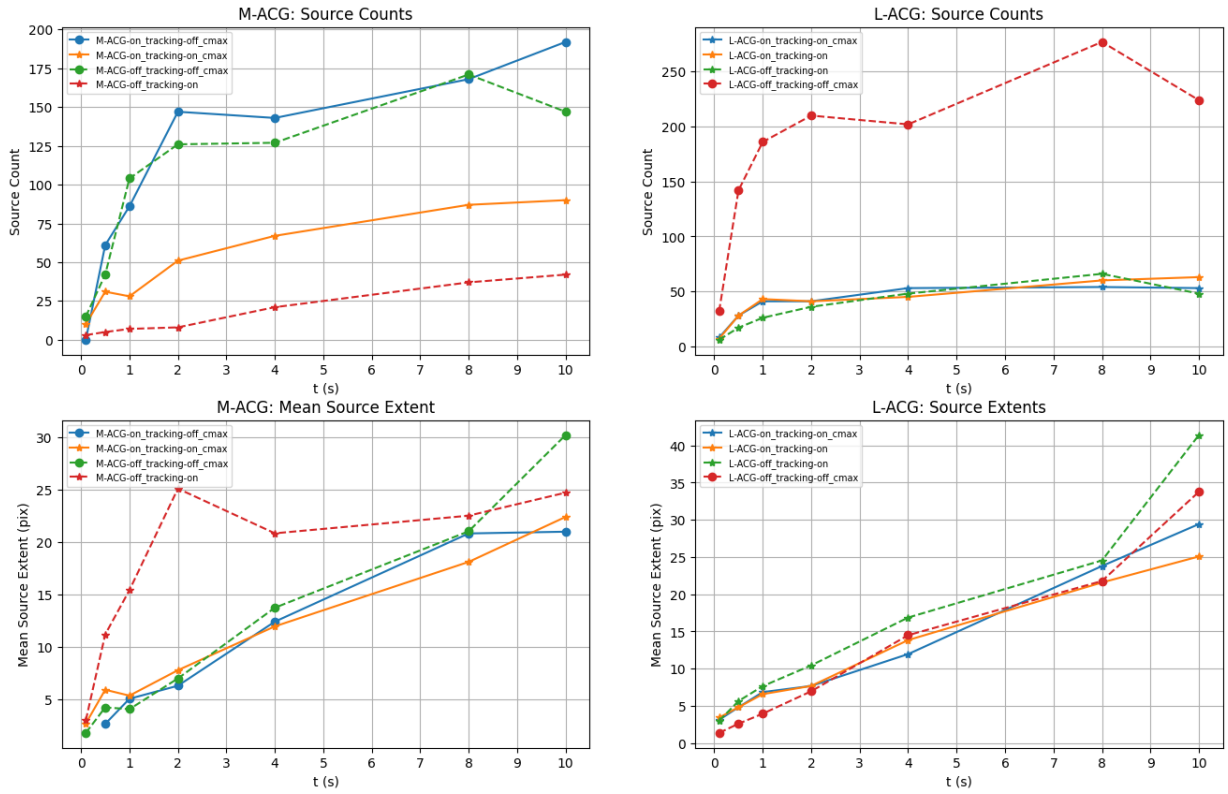

Fig. 10: Comparison of the best performing Mirrored-ACG (left column) and Lensed-ACG (right column) configurations against drift-scanning and tracked observations with detectable source count (top row) and mean detected source extent (bottom row) for exposure times varying from 0.5 seconds to 10 seconds.

is required to fully realise each device's performance. Moreover, to more accurately estimate the appropriate beam steering speed, additional motion caused by wind, mount vibration and atmospheric effects will need to be minimised to isolate only ACG induced motion. Our results further reinforce the notion of an upper bound on the 'pixel speed' of sources in the FOV, beyond which we see a reduction in the sensitivity of the EBS, which was observed in our previous work with the additional relatively random high speed and frequency motion induced by windy conditions reducing the sensitivity of the EBS [16]. In this previous work, our faintest source detections occurred when the mount slew rate was 0.0004 degrees per second (or 1.2 pixel per second of source motion on the pixel array given the pixel scale) [16]. However, the optimal beam steering and focus speed range is not yet found, which could depend on both the sensor and the specific algorithm used to deconvolve the data. At such an optimal beam steering and focus speed, the induced motion would create only enough contrast at the pixel array to detect faint sources at the limit of the EBS sensitivity. In future work, we aim to implement these devices in a closed-loop system to isolate the ACG motion. Such a system could also be used to optimise the beam steering motion in real-time to automatically tune the ACG to the particular imaging task and to scene conditions, such as compensating for wind or with adaptive focus. Additionally, a scanning galvo-mirror beam steering system like the Mirrored-ACG would generally require an F-theta lens to ensure consistent focal length across the entire FOV. In this preliminary work without an F-theta lens, and due to low tolerances in the construction of the Mirrored-ACG, we observe blurring around the edge of the field caused by non-planar surfaces and inconstant focal length. We will attempt to fit such a lens in front of the EBS in the small remaining space of the back focus. We may also use a more developed and Commercial Off-The-Shelf Solution (COTS) 2-axis galvo-mirror beam steering system.

The induced motion produced by the ACGs creates a prior on the features of sources within the field. Noise can be easily filtered as it is random and uncorrelated with the induced motion. Introducing this prior addresses the challenges associated with hot pixels, as rapidly spiking noise pixels, which are now made apparent by their stationary position

when motion is induced. Beam steering an entire scene using an ACG is best suited for an application such as space imaging or aerial observations where targets are the primary source of contrast in a sparse scene against a featureless background. Terrestrial scenes that are dense and complex may produce a large number of events using an ACG as most of the scene is likely to produce events, effectively 'saturating' the camera read-out. The beam steering function of the ACGs bears interesting possibilities for use with micro-lens arrays and Bayer filters, where induced motion can be used to sample source qualities as the light passes over different regions of the image plane's filter mask.

Focusing an EBS is difficult since contrast must be generated while focusing to determine when an image is sharpest. This work demonstrates the Lensed-ACG as an approach to estimate the optimal focus by rapidly sweeping through a range of focal lengths while generating contrast to demonstrate ideal focus visually. This work motivates the need for an algorithm to automatically detect this optimal focus point, such as [11], with telescopes for space imaging.

In star-field observations using the Rowe-Ackermann Schmidt Astrograph (RASA) telescope with the ACGs we encountered artefacts due to diffraction caused by Lensed-ACG obstruction in the telescope aperture, given the RASA design places the image plane at the aperture. These artefacts are most apparent when the Lensed-ACG is in the maximum de-focused position. These effects appear as diffraction spikes, but most notably in the maximum de-focus position, a rough silhouette of the Lensed-ACG in the PSF of bright sources. These artefacts were less prevalent in data collected using the Mirrored-ACG since the obstruction is smaller and the Mirrored-ACG does not deliberately de-focus sources. Future designs will either use a different telescope with a focal plane in the rear of the telescope, or we will aim to reduce the effect of the obstruction by fitting the entire ACG within the existing 92 mm central obstruction which houses the RASAs lenses. The current preliminary design of the Lensed-ACG uses a relatively small 5.8 mm clear aperture, which does not cover the entire Gen 4 HD chip (6.2×3.5 mm^2 detailed in Tab. 1), causing distortion surrounding the field edge. In future work, we will improve this preliminary design with a larger clear aperture lens to avoid this effect. We use default EBS bias settings for all of our recordings in this work since selecting these bias voltages is not trivial and this selection greatly affects the noise properties of the sensor.

4. CONCLUSION

The ACG devices developed and demonstrated in this paper are shown to improve source detection and resolution in EBS observations with artificially generated contrast and address the 'perfect tracking phenomena'. Our Lensed-ACG device is demonstrated to automatically locate optimal focus, solving a difficult problem in event-based space imaging and improving the detection of faint targets. The Mirrored-ACG was also shown to improve source detection and resolving while drift scanning, shown in previous work as an effective technique for observing faint sources using an event-based vision sensor. We aim to continue improving these devices and develop specialised algorithms to process ACG to resolve fainter sources. The ACG imaging techniques developed in this paper provide the space-sensing field with a novel event-based space imaging approach that better serves the goals of space domain awareness by providing accurate and timely information on the space domain with improved sensitivity and target resolving. The outcomes of this paper continue efforts to improve the capabilities of EBSs for use in tracking and space imaging tasks and, therefore, contribute to the growing efforts of the international Space Situational Awareness (SSA) and the development of the event-based technology in astronomy and space science applications.

5. ACKNOWLEDGEMENTS

This study was based in part on data obtained at Western Sydney University (WSU), Penrith Observatory. We acknowledge the traditional owners of the land on which the WSU Penrith Observatory stands, the Dharug people, and pay our respects to elders past and present.

6. REFERENCES

[1] Samya Bagchi and Tat-Jun Chin. Event-based star tracking via multiresolution progressive hough transforms. In *Proceedings of the IEEE/CVF Winter Conference on Applications of Computer Vision*, pages 2143–2152, 2020.

[2] Nicolas Boehrer, Robert PJ Nieuwenhuizen, and Judith Dijk. Turbulence mitigation in imagery including moving objects from a static event camera. *Optical Engineering*, 60(5):053101–053101, 2021.

[3] Tat-Jun Chin, Samya Bagchi, Anders Eriksson, and Andre van Schaik. Star tracking using an event camera. In *Proceedings of the IEEE Conference on Computer Vision and Pattern Recognition Workshops*, pages 0–0, 2019.
[4] Gregory Cohen, Saeed Afshar, and André van Schaik. Approaches for astrometry using event-based sensors. In *Advanced Maui Optical and Space Surveillance (AMOS) Technologies Conference*, page 25, 2018.
[5] Gregory Cohen, Saeed Afshar, André van Schaik, Andrew Wabnitz, Travis Bessell, Mark Rutten, and Brittany Morreale. Event-based sensing for space situational awareness. 11 2017.
[6] Guillermo Gallego, Tobi Delbrück, Garrick Orchard, Chiara Bartolozzi, Brian Taba, Andrea Censi, Stefan Leutenegger, Andrew J Davison, Jörg Conradt, Kostas Daniilidis, et al. Event-based vision: A survey. *IEEE transactions on pattern analysis and machine intelligence*, 44(1):154–180, 2020.
[7] Guillermo Gallego, Henri Rebecq, and Davide Scaramuzza. A unifying contrast maximization framework for event cameras, with applications to motion, depth, and optical flow estimation. In *Proceedings of the IEEE Conference on Computer Vision and Pattern Recognition*, pages 3867–3876, 2018.
[8] Germain Haessig, Xavier Berthelon, Sio-Hoi Ieng, and Ryad Benosman. A spiking neural network model of depth from defocus for event-based neuromorphic vision. *Scientific reports*, 9(1):3744, 2019.
[9] Botao He, Ze Wang, Yuan Zhou, Jingxi Chen, Chahat Deep Singh, and Fei Gao. A texture-enhanced event camera using rotating wedge prism.
[10] Dustin Lang, David W Hogg, Keir Mierle, Michael Blanton, and Sam Roweis. Astrometry. net: Blind astrometric calibration of arbitrary astronomical images. *The astronomical journal*, 139(5):1782, 2010.
[11] Shijie Lin, Yinqiang Zhang, Lei Yu, Bin Zhou, Xiaowei Luo, and Jia Pan. Autofocus for event cameras. In *Proceedings of the IEEE/CVF Conference on Computer Vision and Pattern Recognition*, pages 16344–16353, 2022.
[12] Misha Mahowald. The silicon retina. In *An Analog VLSI System for Stereoscopic Vision*, pages 4–65. 1994.
[13] Julien NP Martel, Lorenz K Müller, Stephen J Carey, Jonathan Müller, Yulia Sandamirskaya, and Piotr Dudek. Real-time depth from focus on a programmable focal plane processor. *IEEE Transactions on Circuits and Systems I: Regular Papers*, 65(3):925–934, 2017.
[14] Abhishek Mishra, Rohan Ghosh, Jose C Principe, Nitish V Thakor, and Sunil L Kukreja. A saccade based framework for real-time motion segmentation using event based vision sensors. *Frontiers in neuroscience*, 11:83, 2017.
[15] Matthias Oster, Patrick Lichtsteiner, Tobias Delbruck, and Shih-Chii Liu. A spike-based saccadic recognition system. In *2007 IEEE International Symposium on Circuits and Systems*, pages 3083–3086. IEEE, 2007.
[16] Nicholas Owen Ralph, Alexandre Marcireau, Saeed Afshar, Nicholas Tothill, André van Schaik, and Gregory Cohen. Astrometric calibration and source characterisation of the latest generation neuromorphic event-based cameras for space imaging. *arXiv preprint arXiv:2211.09939*, 2022.
[17] Cyril Rashbass. The relationship between saccadic and smooth tracking eye movements. *The Journal of physiology*, 159(2):326, 1961.
[18] Peter Senior, Steve Eckersley, Victoria Irwin, Ben Stern, Andrew Haslehurst, Andrew Cawthorne, Alex da Silva Curiel, and Martin Sweeting. Can we use low-cost small satellite to observe space debris missed by ground systems?
[19] Timo Stoffregen and Lindsay Kleeman. Event cameras, contrast maximization and reward functions: An analysis. In *Proceedings of the IEEE/CVF Conference on Computer Vision and Pattern Recognition*, pages 12300–12308, 2019.